Korean J. Chem. Eng., **31**(10), 1859-1864 (2014)
DOI: 10.1007/s11814-014-0132-1

pISSN: 0256-1115
eISSN: 1975-7220

In-situ synthesis of hydrotalcite and its application in separation of simulated radionuclide Eu(III)

Caicun Zha, Xiaoli Sun, Nai Li, and Shaoming Yu†

School of Chemical Engineering, Hefei University of Technology, Hefei, 230009, Anhui, China
(*Received 19 January 2014 • accepted 1 May 2014*)

Abstract−The simulated radionuclide Eu(III) was separated effectively by using the in-situ synthesis of hydrotalcite. The optimal conditions of pH, Mg/(Eu+Al) molar ratio, and initial Eu(III) concentration for separating Eu(III) and achieving a single hydrotalcite phase were investigated systematically and determined to be 10, 3.0, and 600 mg L^{-1}, respectively. Under the optimal separation conditions, the removal percentage of Eu(III) reached 99.8%. The characterization results suggested that Eu(III) was incorporated into the crystal lattice of hydrotalcite completely and fully immobilized in the structure of spinel by calcining, and the morphology of the synthetic hydrotalcite containing Eu(III) was in hexagonal platelet-like sheet.

Keywords: High Level Liquid Waste, Separation, Hydrotalcite, In-situ Synthesis, Europium

INTRODUCTION

The decarbonization of electricity generation process has been promoted by the increasing awareness of global climate changes, rising level of green house gases, and depleting reserves of fossil fuel. As a carbon neutral energy, nuclear energy appears to be the most viable option to meet the increasing demand of energy [1]. However, the expanding of the nuclear power industry is accompanied with increasing accumulation of high level liquid waste (HLLW), which is produced from the reprocessing of spent nuclear fuel. Some long-lived minor actinides like ^{243}Am(III), ^{244}Cm(IV), and specific fission product elements like ^{90}Sr(II), ^{137}Cs(I), ^{99}Tc(VII), and ^{129}I can be found in the HLLW [2,3]. These radionuclides are permanently hazardous to humans, plants, and animals because of their persistent long-life radioactivity and biological toxicity. The accident at the Fukushima Daiichi Nuclear Power Plant caused by the Great East Japan Earthquake of March 11, 2011 reminded us of the seriously disastrous consequence from the release of radioactive substances over a wide range [4], and warned us that it is of great significance to treat the radionuclides in the HLLW before they are discharged into the environment, which is crucial to achieve sustainable development of nuclear energy [5,6]. Therefore, an effective method for the safe treatment and disposal for the HLLW should be developed as soon as possible.

The major considerations of the safe treatment and disposal for the HLLW are to ensure its isolation from the biosphere and prevent any significant release of radionuclides. During the treatment and disposal for the HLLW, the radionuclides must be separated first and then immobilized in a highly stable solid. Thereafter, the solids must be stored in a secure, long-term repository. An effective method to separate radionuclides from the HLLW is to make them water insoluble by fixing them in solid matrix materials called synthetic rocks (synroc) [7]. Synroc is generally considered as a low-risk tailored waste form offering higher waste loading and overall cost savings, which is also the most effective and durable means for immobilizing various forms of the HLLW for safe treatment and disposal [8]. Several methods like ion exchange [9] and solvent extraction [10] have been developed to separate radionuclides from the HLLW. As the HLLW contains miscellaneous ions and substantial amount of acid, ion exchange is not considered as a good choice because of its poor selectivity and slow adsorption kinetics [11]. Currently, the most commonly used method is solvent extraction. Even though it shows high selectivity and extraction ability for radionuclides, and the radionuclides can be separated effectively, a large amount of secondary organic waste is usually generated at the same time, and the separated radionuclides cannot be preserved for long-term conservation [12].

Synthetic hydrotalcite-like compounds (HTlcs) are layered double hydroxides with the general formula $[M^{II}_{1-x}M^{III}_{x}(OH)_2]^{x+}(A^{n-})_{x/n}\cdot mH_2O$ [13,14], where M^{II} (often Mg^{II}) and M^{III} (often Al^{III}) are divalent and trivalent cations, respectively, and A^{n-} (often CO_3^{2-}) represents interlayer anions (Fig. 1) [15]. According to the principle of

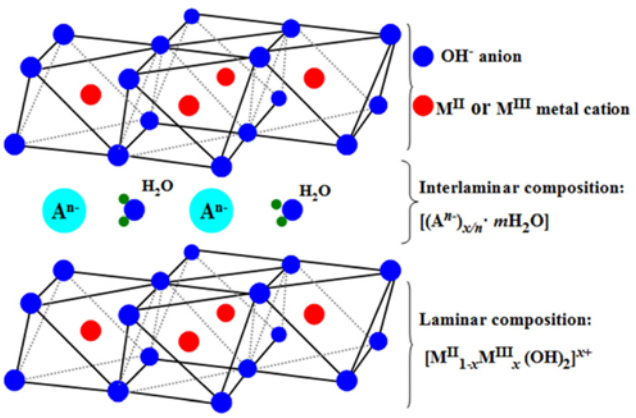

Fig. 1. Schematic representation of HTlc structure.

†To whom correspondence should be addressed.
E-mail: shmyu@hfut.edu.cn
Copyright by The Korean Institute of Chemical Engineers.

isomorphous substitution, some cations like Eu(III) [16], La(III) [17], and Ce(III) [18] can substitute for Mg^{II} or Al^{III} and enter the crystal lattice of hydrotalcite. Therefore, it is theoretically possible to separate some radionuclides from the HLLW using in-situ synthesis of hydrotalcite. Previous studies have demonstrated that hydrotalcite may incorporate a wide range of trace elements and radionuclides [19,20]. When HTlcs are calcined above 600 °C, stable phases of $M^{II}M^{III}{}_2O_4$ (spinel) and $M^{II}O$ can be formed [21]. Spinel is one of the main synroc components for radionuclide immobilization [22]. The radionuclides substituting for Mg^{II} or Al^{III} incorporated into the crystal lattice of hydrotalcite can be immobilized in the structure of spinel by calcining. After that, the spinel with radionuclides in the structure can be isolated from the biosphere by being deeply buried for long-term preservation.

$^{152+154}$Eu is one of the most hazardous contaminants in radioactive wastewater because of its relatively high energy (hard γ-emitter) and long half-life. It has a similar physicochemical behavior to that of trivalent lanthanides and actinides, because its ionic radius is similar. Based on this, Eu(III) is used as the homologue for trivalent actinides [6] to avoid the direct damage of radiation, and our efforts have been directed to separate simulated radionuclide Eu(III) as a contribution to the safe treatment and disposal for radionuclides in the HLLW. The main aim of our present study was to investigate the feasibility of separating Eu(III) by using in-situ synthesis of hydrotalcite and obtain a single hydrotalcite phase. The effect of pH, Mg/(Eu+Al) molar ratio (r), and initial Eu(III) concentration (C_{Eu}) on the separation efficiency was studied systematically to ascertain the optimal conditions for the separation of Eu(III). The samples of Eu(III) doped hydrotalcite (Eu-HTlc) were characterized by X-ray diffraction (XRD), Fourier transform infrared spectroscopy (FT-IR), and scanning electron microscopy (SEM), the calcined Eu-HTlc were characterized by XRD, SEM, and energy dispersive spectrometer (EDS). The phase assemblages of Eu-HTlc and its calcined sample are briefly discussed.

EXPERIMENT

1. Materials

All chemicals were analytical grade and used without further purification. $Mg(NO_3)_2\cdot 6H_2O$, $Al(NO_3)_3\cdot 9H_2O$, and $Eu(NO_3)_3\cdot 6H_2O$ were used as the sources for Mg(II), Al(III), and Eu(III), respectively.

2. Synthesis of Eu-HTlc

A series of Eu-HTlc samples were prepared by in-situ synthesis of hydrotalcite according to the following typical procedures.

Two solutions, A and B, were prepared. Solution A was prepared by dissolving mixed nitrates of Mg(II), Al(III), and Eu(III) with a predefined ratio in deionized water. Solution B was prepared with NaOH and Na_2CO_3 dissolving in deionized water according to the formulas $[OH^-]=2([Mg(II)]+[Al(III)]+[Eu(III)])$ and $[CO_3^{2-}]=0.5([Al(III)]+[Eu(III)])$. Solution B was added dropwise into solution A under vigorous stirring until the pH of resultant solution was adjusted to an assigned value [18,23], and then the resulting precipitation obtained was transferred into a Teflon-lined stainless steel autoclave for hydrothermal treatment at 120 °C for 12 h [24]. After hydrothermal treatment, the precipitate was filtered and washed thoroughly with hot distilled water until the pH of filtrate reached about 7. The filtrate was collected and analyzed to determine the concentration of residual Eu(III) using spectrophotometric methods, and then the removal percentage of Eu(III) was calculated. The washed filtration cakes were collected and dried in the open air at 80 °C for 12 h. Some dried samples were prepared for the characterizations of XRD, FT-IR, and SEM to investigate the separation efficiency at different pH, r, and initial C_{Eu}, and to ascertain the optimal conditions for the separation of Eu(III). The others were calcined at 1,100 °C for 5 h and then characterized by XRD, SEM, and EDS.

3. Characterization Methods

XRD patterns were collected on a DX-2700 X-ray diffractometer using Cu $K\alpha$ radiation. The FT-IR spectrum was recorded on a THERMO NICOLET67 spectrophotometer using KBr pellet technique. The SEM micrograph of Eu-HTlc was performed on a JEOL JSM-6700F instrument at an acceleration voltage of 5.0 kV and a working distance of 5.9 mm, while the SEM micrograph of calcined Eu-HTlc was performed on an SU8200 instrument at an acceleration voltage of 15.0 kV and a working distance of 14.6 mm.

RESULTS AND DISCUSSION

1. Influence of pH on the Synthesis of Eu-HTLc

The pH of the synthesis environment plays a key role in the separation efficiency of Eu(III) and directly determines whether the synthesized hydrotalcite has a single crystal phase or not. In the experiment, a mixed solution containing Mg(II), Al(III), and Eu(III) with a predefined ratio was titrated by the solution of NaOH (1.0 mol L^{-1}) at a constant rate under vigorous stirring. During the titration, pH increased with the addition of NaOH, and precipitation gradually formed in the solution and the titration curve, i.e., the variation plot of pH versus the amount of NaOH added, was obtained, as shown in Fig. 2 [25].

Three plateaus of pH can be found in the ranges of 2.8-4.3, 7.8-11.0, and 13.3-14.0 in the figure. The first plateau is attributed to the hydrolization and polymerization of Al(III). As Mg(II) consumes OH^-, and then $Mg(OH)_2$ participates in the formation of hydrotalcite, the pH of solution does not change very much, this results in the formation of the second plateau. After all of the $Mg(OH)_2$ is utilized in the formation of hydrotalcite, does the pH begin to rise

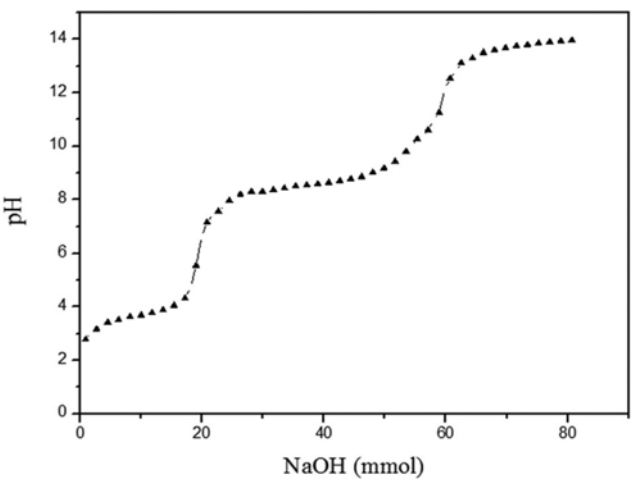

Fig. 2. Titration curves of Mg/Al/Eu mixed nitrate solution (r=3.0, C_{Eu}=600 mg L^{-1}).

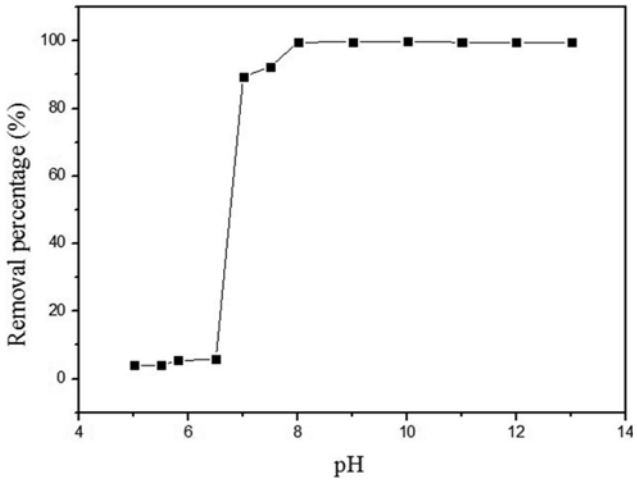

Fig. 3. Influence of pH on the removal percentages of Eu(III) (r= 3.0, C_{Eu}=600 mg L^{-1}).

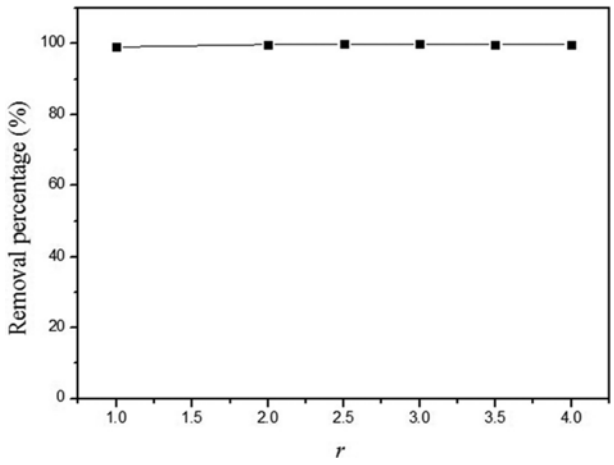

Fig. 5. Influence of r on the removal percentages of Eu(III) (pH= 10, C_{Eu}=600 mg L^{-1}).

again. The appearance of a third plateau corresponds to the pH of solution is closed to that of NaOH solution. Therefore, the optimal range of pH for the synthesis of hydrotalcite is from 7.8 to 11.0.

2. Influence of pH on the Separation Efficiency of Eu(III)

The influence of pH on the removal percentages of Eu(III) is shown in Fig. 3. It can be concluded that the removal percentages are almost unaffected by pH at the range of 8-11. The precipitation pH of Eu(III) is between 7 and 8. When pH is 7, the removal percentage is 89.5%, which is due to Eu(III) remaining in solution instead of entering the crystal lattice of hydrotalcite beginning to precipitate at the pH of 7, but not completely; when pH is 8-11, the removal percentages are above 99%, which is assigned to the synthesis pH being higher than the precipitation pH of Eu(III); all the Eu(III) which are not incorporated into the crystal lattice of hydrotalcite exist in the state of precipitation.

The XRD patterns of Eu-HTlc samples synthesized at different pH (Fig. 4) clearly show the characteristic reflections of hydrotalcite (JCPDS-35-0965) (i) sharp and intense basal 00*l* reflections of 003 and 006 planes in the low angle region (2θ<25°), (ii) broad 0*kl* reflections of 012, 015, and 018 planes in the middle angle region (2θ=30°-50°), and(III) sharp *hk*0 and *hkl* reflections of 110 and 113 planes in the high angle region (2θ=55°-65°). These sharp and symmetric peaks (110 and 113) confirm the formation of a single well-crystallized hydrotalcite [26]. Some diffraction peaks of impurities such as $Eu(OH)_3$ (JCPDS-17-0781) and EuOOH (JCPDS-18-0510) can be observed when the synthesis pH is 8, 9, and 12. The presence of EuOOH and $Eu(OH)_3$ demonstrates that the separated Eu(III) is not incorporated into the crystal lattice of hydrotalcite completely. EuOOH and $Eu(OH)_3$ will be transformed into Eu_2O_3 by calcining, which may result in an unwanted increase of the elemental normalized leach rate of Eu(III) in the leaching tests. Since the main objective of our study was to achieve a higher removal percentage of simulated radionuclide and obtain a single hydrotalcite phase, the optimal range of pH was chosen to be from 10 to 11. Furthermore, in order to reduce the dosage of alkali and make the experimental condition more moderate, 10 was identified as the optimal pH for the separation of Eu(III).

3. Influence of r on the Separation Efficiency of Eu(III)

The influence of r on the removal percentages of Eu(III) is presented in Fig. 5. No apparent differences of the removal percentages can be found, which can be attributed to the synthesis pH

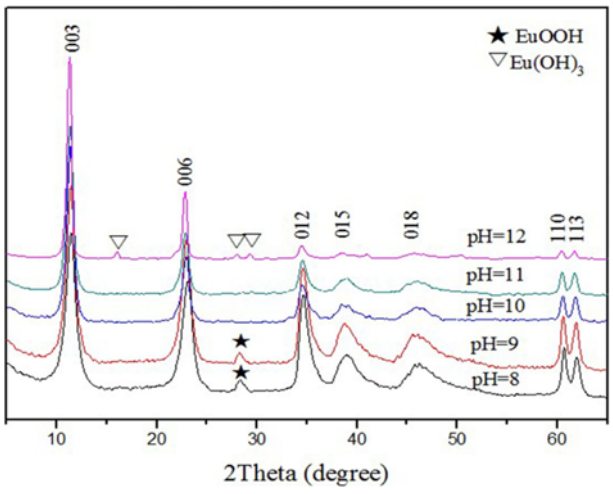

Fig. 4. XRD patterns of Eu-HTlcs synthesized at different pH.

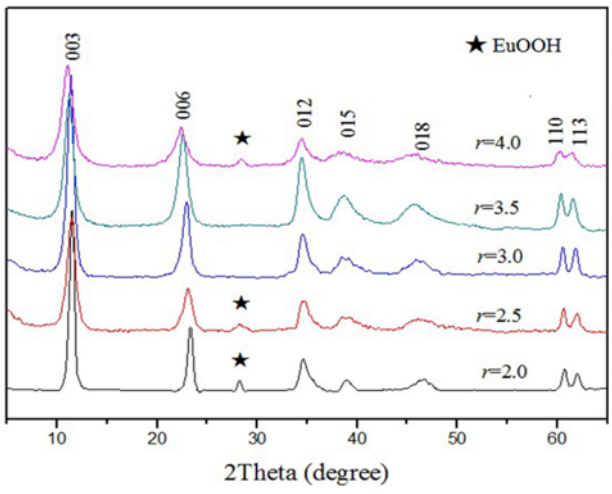

Fig. 6. XRD patterns of Eu-HTlcs synthesized at different r.

being higher than the precipitation pH of Eu(III). Eu(III) either enters the crystal lattice of hydrotalcite or exists in the form of a hydroxy- or oxyhydroxy- precipitate.

All of the XRD patterns of Eu-HTlc samples synthesized at different r exhibit features of a highly crystalline hydrotalcite phase (Fig. 6). In these diffraction diagrams, the diffraction signals of EuOOH (JCPDS-18-0510) can be observed when r is 2.0, 2.5, and 4.0. Meanwhile, when r is 3.0 or 3.5, single hydrotalcite phase is found without any other impurity phases. Therefore, r must be fixed to 3.0 or 3.5 for obtaining a single hydrotalcite phase.

4. Influence of Initial C_{Eu} on the Separation Efficiency of Eu(III)

The influence of initial C_{Eu} on the removal percentages of Eu(III) shown in Fig. 7 suggests the removal percentages are almost the same, which is because the synthesis pH is higher than the precipitation pH of Eu(III). Under this pH condition, similar to the cases in section 3.3, no matter how much the initial Eu(III) is, Eu(III) will stay in the form of precipitation in solution if not be incorporated into the crystal lattice of hydrotalcite.

The XRD patterns of Eu-HTlc samples synthesized at different initial C_{Eu} are displayed in Fig. 8. When the initial C_{Eu} is above 600 mg L^{-1}, the diffraction signals of impurities like $Al(OH)_3$ (JCPDS-20-0011) and EuOOH (JCPDS-18-0510) can be observed. Furthermore, the intensity of the EuOOH diffraction signal increases with the initial C_{Eu}, which clearly indicates more and more Eu(III) are not incorporated into the crystal lattice of hydrotalcite. Therefore, 600 mg L^{-1} is selected as the optimal initial C_{Eu} for obtaining a single hydrotalcite phase and increasing the amount of Eu(III) to be incorporated into the crystal lattice of hydrotalcite as much as possible. When C_{Eu} is 600 mg L^{-1}, the molar ratio of Mg/Al/Eu is calculated to be 3/0.96/0.04 as shown in Table 1, in which the molar ratios of Mg/Al/Eu with different initial C_{Eu} are listed.

Hydrotalcite belongs to a hexagonal system; therefore, the lattice parameters a (distance between cations) and c (spacing between layers) can be calculated according to the formulas $a=2d_{110}$ and $c=3d_{003}$ [27]. Based on the changes of a and c, it can be ascertained whether Eu(III) enters crystal lattice of hydrotalcite or not. The lattice parameters of Eu-HTlcs synthesized under different initial C_{Eu} are calculated and presented in Table 2. According to the table, the lattice parameters a and c increase with the initial C_{Eu} can be found, which is the result of Eu(III) substituting for Mg (II) and Al(III) entering the crystal lattice of hydrotalcite, and the ionic radius of Eu(III) is

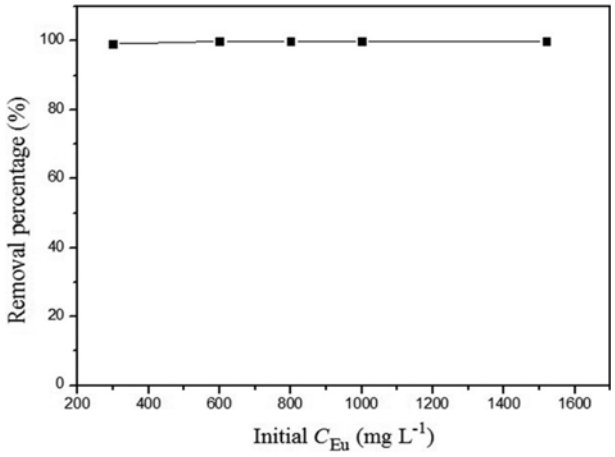

Fig. 7. Influence of initial C_{Eu} on the removal percentages of Eu(III) (pH=10, r=3.0).

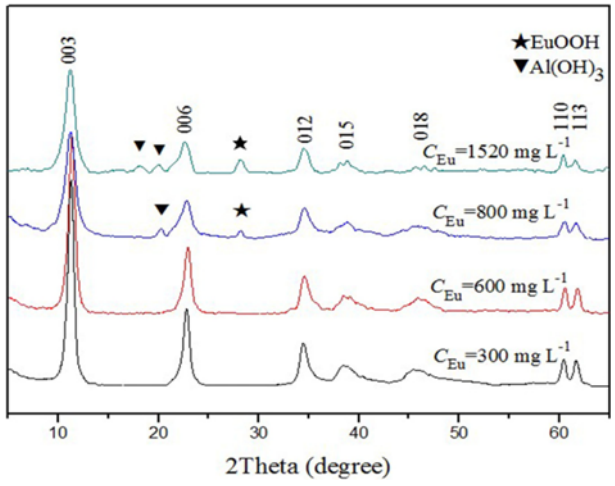

Fig. 8. XRD patterns of Eu-HTlcs synthesized at different initial C_{Eu}.

Table 1. Molar ratios of Mg/Al/Eu at different initial C_{Eu}

Samples	Initial C_{Eu} (mg L^{-1})	Molar ratios of Mg/Al/Eu
HTlc-1	300	3/0.98/0.02
HTlc-2	600	3/0.96/0.04
HTlc-3	800	3/0.95/0.05
HTlc-4	1520	3/0.90/0.10

Table 2. Crystallographic parameters of Eu-HTlcs of varying initial C_{Eu}

Samples	Initial C_{Eu} (mg L^{-1})	a (Å)	c (Å)
HTlc-0	0	3.0512	23.1657
HTlc-1	300	3.0552	23.3478
HTlc-2	600	3.0566	23.4084
HTlc-3	800	3.0582	23.4132
HTlc-4	1520	3.0596	23.4714

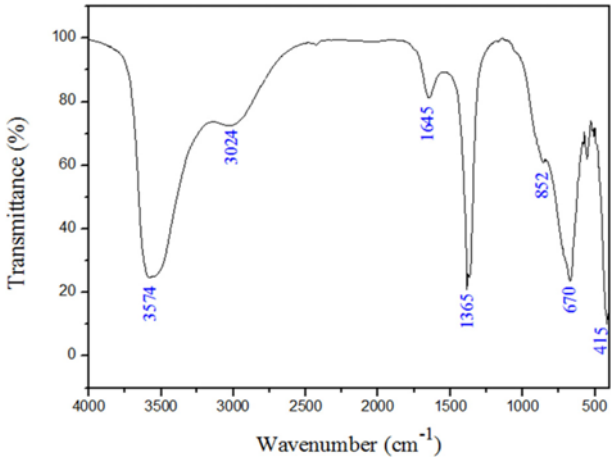

Fig. 9. FT-IR spectrum of Eu-HTlc.

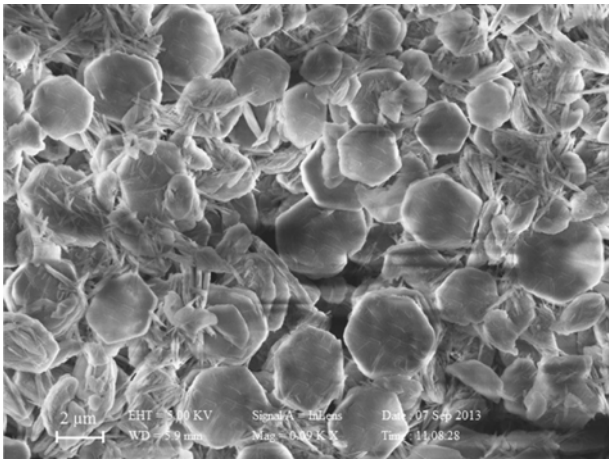

Fig. 10. SEM micrograph of Eu-HTlc.

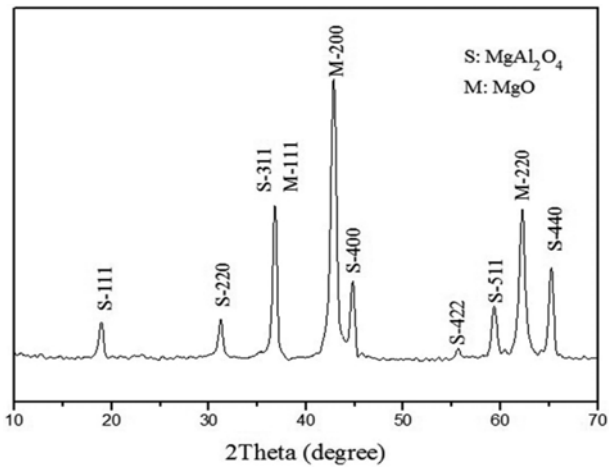

Fig. 11. XRD pattern of calcined Eu-HTlc.

bigger than theirs. The ionic radius of Mg(II), Al(III), and Eu(III) is 0.72 Å, 0.535 Å, and 0.947 Å, respectively.

5. Characterizations of Eu-HTlc

Fig. 9 displays the FT-IR spectrum of Eu-HTlc synthesized under the optimal conditions (pH=10, r=3.0, and C_{Eu}=600 mg L^{-1}) determined above. A typical FT-IR spectrum of hydrotalcite is presented. The broad peak around 3,574 cm^{-1} is attributed to the stretching vibration of structural O-H groups hydrogen bonded with interlamellar water or O-H groups in adjacent layers [28]. The shoulder at 3,024 cm^{-1} is attributed to H-bonded stretching vibration. The shoulder peak at 1,645 cm^{-1} is the characteristic band of H_2O, which should be assigned to the adsorbed water molecules in the interlayer. The sharp intense vibrational peak of carbonates at 1,365 cm^{-1} could be attributed to the ν_3 stretching mode of the interlayer carbonate anions in a symmetric environment, and the two peaks close to 852 cm^{-1} and 670 cm^{-1} are due to the ν_2 and ν_4 modes of the interlayer carbonate group, respectively. The typical peak of hydrotalcite (HO-Mg-Al-OH) appears at 415 cm^{-1} [24,29,30].

In Fig. 10, the particles of Eu-HTlc synthesized under the optimal separation conditions are in hexagonal platelet-like sheets with an average plate diameter of 2.0 μm as reported previously [31], which suggests the structure of hydrotalcite is not modified by the incorporation of Eu(III).

6. Characterization of Calcined Eu-HTlc

The XRD pattern of calcined Eu-HTlc obtained from Eu-HTlc synthesized under the optimal separation conditions and calcined at 1,100 °C for 5 h is presented in Fig. 11. The peaks at 19.1° (S-111), 31.3° (S-220), 36.9° (S-311), 44.9° (S-400), 55.6° (S-422), 59.4° (S-511), and 65.3° (S-440) should be assigned to the characteristic diffraction peaks of $MgAl_2O_4$ (JCPDS-21-1152). The presence of the characteristic diffraction peaks of MgO (JCPDS-45-0946) in the pattern is assigned to the excess of Mg(II). The separated Eu(III) is incorporated into the crystal lattice of hydrotalcite completely and fully immobilized in the structure of spinel by calcining as demonstrated by the absence of Eu_2O_3.

The SEM micrograph and EDS spectrum of calcined Eu-HTlc are shown in Fig. 12(a) and Fig. 12(b), respectively. The micrograph of SEM shows a smooth platelet morphology of the calcined Eu-HTlc, and the existence of Eu(III) in the calcined Eu-HTlc is confirmed by the EDS spectrum. Combining with the XRD pattern of calcined Eu-HTlc, it can be concluded that Eu(III) is immobilized in the structure of spinel.

CONCLUSIONS

Simulated radionuclide Eu(III) was separated with a high removal percentage, and a single hydrotalcite phase was obtained by in-situ synthesis of hydrotalcite. The optimal separation conditions (pH=10, r=3.0, and initial C_{Eu}=600 mg L^{-1}) were determined by a series of single factor tests and XRD analysis. Not only could Eu(III) be

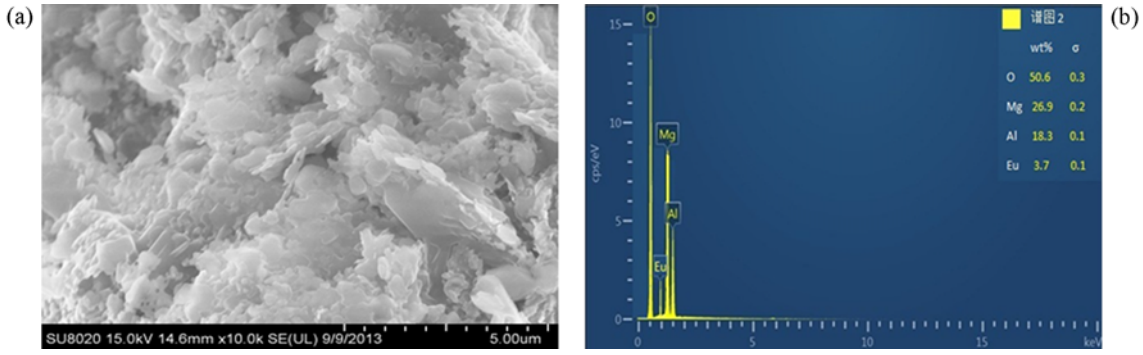

Fig. 12. SEM micrograph and EDS spectrum of calcined Eu-HTlc.

separated with a high removal percentage (99.8%), but also incorporated into the crystal lattice of hydrotalcite completely under these conditions. The morphology of Eu-HTlc was in hexagonal platelet-like sheet and the sizes of particles were about 2 μm. The calcined Eu-HTlc consisted of $MgAl_2O_4$ and MgO without Eu_2O_3 and the content of Eu(III) was 3.7 wt%, which confirmed that Eu(III) incorporated into the crystal lattice of hydrotalcite was immobilized in the structure of spinel by calcining. In all, simulated radionuclide Eu(III) was separated successfully by in-situ hydrotalcite synthesis. Therefore, this method would have potential applications in the safe treatment and disposal for radionuclides in the HLLW.

ACKNOWLEDGEMENT

Financial support from National Natural Science Foundation of China (20971033) is acknowledged.

REFERENCES

1. C. S. Kedari, S. S. Pandit and P. M. Gandhi, *J. Membr. Sci*., **430**, 188 (2013).
2. A. Y. Zhang, E. Kuraoka and M. Kumagai, *Sep. Purif. Technol*., **50**(1), 35 (2006).
3. B. Krishna, S. Rao, J. Arunachalam, M. Murali, S. Kumar and V. Manchanda, *Sep. Purif. Technol*., **38**(2), 149 (2004).
4. D. Rana, T. Matsuura, M. A. Kassim and A. F. Ismail, *Desalination*, **321**, 77 (2013).
5. S. W. Li, J. Chen and J. C. Wang, *J. Radioanal. Nucl. Chem*., **292**(2), 697 (2012).
6. M. R. Mahmoud and H. H. Someda, *J. Radioanal. Nucl. Chem*., **292**(3), 1391 (2012).
7. H. Abe, A. Satoh, K. Nishida, E. Abe, T. Ncaka, M. Imai and H. Kitazawa, *J. Solid State Chem*., **179**(5), 1521 (2006).
8. H. S. Potdar, S. Vijayanand, K. K. Mohaideen, K. R. Patil, P. A. Joy, R. R. Madhavan, K. V. G. Kutty, R. D. Ambashta and P. K. Wattal, *Mater. Chem. Phys*., **123**(2-3), 695 (2010).
9. S. H. Lee, J. H. Yoo and J. H. Kim, *Korean J. Chem. Eng*., **21**(5), 1038 (2004).
10. A. Dakshinamoorthy, P. S. Dhami, P. W. Naik, N. L. Dudwadkar, S. K. Munshi, P. K. Dey and V. Venugopal, *Desalination*, **232**(1-3), 26 (2008).
11. F. F. Bai, G. Ye, G. J. Chen, J. C. Wei, J. C. Wang and J. Chen, *React. Funct. Polym*., **73**(1), 228 (2013).
12. S. H. Tan, X. G. Chen, Y. Ye, J. Sun, L. Q. Dai and Q. Ding, *J. Hazard. Mater*., **179**(1-3), 559 (2010).
13. Y. M. Yang, X. F. Zhao, Y. Zhu and F. Z. Zhang, *Chem. Mater*., **24**(1), 81 (2012).
14. O. D. Pavel, D. Tichit and I. C. Marcu, *Appl. Clay Sci*., **61**, 52 (2012).
15. R. Salomao, L. M. Milena, M. H. Wakamatsu and V. C. Pandolfelli, *Ceram. Int*., **37**(8), 3063 (2011).
16. T. Stumpf, H. Curtius, C. Walther, K. Dardenne, K. Ufer and T. Fanghanel, *Environ. Sci. Technol*., **41**(9), 3186 (2007).
17. X. M. Fan, Z. H. Yang, X. Xie, W. Long, R. J. Wang and Z. L. Hou, *J. Power Sources*, **241**, 404 (2013).
18. J. Das, D. Das and K. M. Parida, *J. Colloid Interface Sci.*, **301**(2), 569 (2006).
19. G. B. Douglas, L. A. Wendling, R. Pleysier and M. G. Trefry, *Mine Water Environ*., **29**(2), 108 (2010).
20. G. Douglas, M. Shackleton and P. Woods, *Appl. Geochem*., **42**, 27 (2014).
21. W. Ma, N. N. Zhao, G. Yang, L. Y. Tian and R. Wang, *Desalination*, **268**(1-3), 20 (2011).
22. A. Ringwood, S. Kesson, N. Ware, W. Hibberson and A. Major, *Nature*, **278**, 219 (1979).
23. B. M. Choudary, V. S. Jaya, B. R. Reddy, M. L. Kantam, M. M. Rao and S. S. Madhavendra, *Chem. Mater*., **17**(10), 2740 (2005).
24. S. K. Sharma, P. K. Kushwaha, V. K. Srivastava, S. D. Bhatt and R. V. Jasra, *Ind. Eng. Chem. Res*., **46**(14), 4856 (2007).
25. K. Yan, X. M. Xie, J. P. Li, X. L. Wang and Z. Z. Wang, *J. Nat. Gas Chem*., **16**(4), 371 (2007).
26. U. Sharma, B. Tyagi and R. V. Jasra, *Ind. Eng. Chem. Res*., **47**(23), 9588 (2008).
27. A. Serrano-Lotina, L. Rodriguez, G. Munoz and L. Daza, *J. Power Sources*, **196**(9), 4404 (2011).
28. D. Zhao, Y. Wang, H. Xuan, Y. Chen and T. Cao, *J. Radioanal. Nucl. Chem*., **295**(2), 1251 (2013).
29. P. Zhang, S. Sago, T. Yamaguchi and G. M. Anilkumar, *J. Power Sources*, **230**, 225 (2013).
30. Y. J. Feng, D. Q. Li, Y. Wang, D. G. Evans and X. Duan, *Polymer Degradation and Stability*, **91**(4), 789 (2006).
31. M. Ogawa and H. Kaiho, *Langmuir*, **18**(11), 4240 (2002).